An Ultrasound-Driven Kinematic Model of the Heart That Enforces Local Incompressibility

Dan Lin, Jeffrey W. Holmes, and John A. Hossack

Department of Biomedical Engineering,
University of Virginia, Charlottesville, Virginia, USA
{dl7ac,holmes,jh7fj}@virginia.edu

Abstract. Local incompressibility can be used to improve fitting and analysis of ultrasound-based displacement data using a heart model. An analytic mathematical model incorporating inflation, torsion, and axial extension was generalized for the left ventricle. Short-axis and long-axis images of mouse left ventricles were acquired using high frequency B-mode ultrasound and myocardial displacements were determined using speckle tracking. Deformation gradient components in the circumferential and longitudinal directions were fitted using linear regressions. The slopes of these lines were then used to predict motion in the radial directions. The optimized kinematic model accurately predicted the motion of mouse left ventricle during filling with normalized root mean square error of 4.4±1.2%.

1 Introduction

While diagnoses and therapies for cardiovascular diseases (CVD) have improved in recent years, CVD remain a major global health concern. In the United States, heart disease is the leading cause of death, accounting for 33.6% of all deaths in 2007 [1]. In an effort to curtail CVD mortality, patient-specific left ventricular (LV) modeling has been introduced to facilitate improved and individualized diagnoses [2,3,4]. Unfortunately, patient-specific modeling is currently a labor-intensive process, involving multiple medical imaging modalities (typically magnetic resonance imaging (MRI) and computed tomography (CT)), and detailed geometric modeling using finite element analysis (FEA) that requires extensive manual tracings. Thus, current approaches to patient-specific modeling are very expensive. We therefore sought a modeling approach to fitting and interpreting ultrasound data that could provide some of the advantages of patient-specific FEA, such as incorporating known aspects of myocardial mechanics, without requiring detailed knowledge of fiber structure, material properties, etc., for each heart.

Models using simple geometric shapes appropriate to the LV have been influential in studying cardiac mechanics. Cylindrical models have been used to predict distribution of stress and strain around the myocardium [5]. They have also been used to estimate material properties of the myocardium [6]. While these models have been instrumental in understanding regional ventricular function,

D.N. Metaxas and L. Axel (Eds.): FIMH 2011, LNCS 6666, pp. 129–136, 2011.

they are only accurate at the mid-ventricular section of the LV and are inadequate in modeling regions near the apex. Other models using prolate spheroidal and actual heart geometries have had better success in describing motion near the apex as well as other modes of motion observed in LV that cannot be modeled with a cylinder [7].

While there is a plethora of established cylindrical heart models [6,8], existing models are similar in that the radial motion is often assumed to be uniform and axisymmetric around the myocardium. In this paper, we derive a kinematic model describing myocardial deformation using a classic cylindrical model and myocardial incompressibility. We then generalize the model by using actual heart geometry to allow radial motion to vary as a function of R, Θ and Z. This formulation allows more freedom in describing cardiac motion but retains the incompressibility of myocardium as a constraint on the fitted displacement field.

In addition to studying cardiac mechanics, geometric models can also operate as a filter by imposing geometric constraints on allowed myocardial motion. This can be used to discard and correct improbable motion estimates derived from motion tracking techniques. For example, the incompressibility constraint has been used to improve both automated segmentation [9,10] and motion estimation [11,12,13]. This is particularly useful in small animal imaging using ultrasound, where motion estimates using speckle tracking techniques are often noisy. In mouse heart imaging, high heart rate and associated low number of image frames per cardiac cycle can result in significant decorrelation between frames. Additionally, signal dropout, attenuation and anatomical related artifacts (e.g. sternum, rib or lung related multipath reverberation) can also degrade image quality. Under these scenarios, motion estimates are frequently inaccurate and unreliable. While there are disadvantages in using ultrasound images, there exist many post image processing techniques to partially compensate for poor image quality, including clutter and artifact reduction using finite impulse response (FIR) filters [14] and principal component analysis via blind source separation method [15]. Compared to MRI and CT, medical ultrasound imaging is inexpensive, radiation free, and has high temporal image resolution. For these reasons, patient-specific modeling may therefore be feasible in a clinical setting.

2 Methods

2.1 Model Formulation

A general form of cylindrical model describing inflation, torsion and extension of a deformable thick-walled cylinder was adopted from Adkins [16]. A cylinder can inflate and deflate radially, corresponding to LV expansion from end-systole (ES) to end-diastole (ED) and LV contraction from ED to ES, respectively. Simple torsion occurs on the plane perpendicular to the axis of the cylinder, and axial extension and compression along the axis of the cylinder. In the initial cylinder

model, undeformed and deformed states were defined at ES and ED, respectively. Left ventricular filling from ES to ED is simulated using equation (1):

$$r = r(R), \theta = \theta(\Theta) + \tau Z, z = z(Z). \tag{1}$$

(R,Θ,Z) and (r,θ,z) are the radial, circumferential and longitudinal components in undeformed and deformed cylindrical coordinates, respectively. During filling, the LV expands radially as a function of R; twists circumferentially as a function of Θ and proportionally to Z by constant τ; and extends longitudinally as a function of Z. We generalized this model to account for spatial nonuniformity expected in an actual heart due to mismatch between the assumed (cylindrical) and actual geometry, regional ischemia, dyssynchrony, etc. Specifically, we allowed radial inflation to vary with circumferential and longitudinal coordinates:

$$r = r(R, \Theta, Z), \theta = \theta(\Theta, Z), z = z(Z). \tag{2}$$

LV deformation from ES to ED can be described using a deformation gradient tensor. In cylindrical polar coordinates and using equation (2), the deformation gradient matrix, F, is [17]:

$$F = \begin{pmatrix} \frac{\partial r}{\partial R} & \frac{1}{R}\frac{\partial r}{\partial \Theta} & \frac{\partial r}{\partial Z} \\ r\frac{\partial \theta}{\partial R} & \frac{r}{R}\frac{\partial \theta}{\partial \Theta} & r\frac{\partial \theta}{\partial Z} \\ \frac{\partial z}{\partial R} & \frac{1}{R}\frac{\partial z}{\partial \Theta} & \frac{\partial z}{\partial Z} \end{pmatrix} = \begin{pmatrix} \frac{\partial r}{\partial R} & \frac{1}{R}\frac{\partial r}{\partial \Theta} & \frac{\partial r}{\partial Z} \\ 0 & \frac{r}{R}\frac{\partial \theta}{\partial \Theta} & r\frac{\partial \theta}{\partial Z} \\ 0 & 0 & \frac{\partial z}{\partial Z} \end{pmatrix}. \tag{3}$$

To find a closed form solution to equation (2), the myocardium is assumed to be incompressible. This is a reasonable assumption since the myocardium is composed of 80% water [18,19], and water is almost perfectly incompressible. While studies have shown that myocardial volume is not isovolumetric due to blood perfusion in the heart, the change in volume is no more than 4% [20]. Using incompressibility, the determinant of the deformation gradient matrix is equal to unity:

$$\det(F) = \left(\frac{\partial r}{\partial R}\right)\left(\frac{r}{R}\frac{\partial \theta}{\partial \Theta}\right)\left(\frac{\partial z}{\partial Z}\right) = 1. \tag{4}$$

Integrating equation (4) and applying boundary condition at the endocardium gives:

$$r(R, \Theta, Z) = \sqrt{\frac{R^2 - R_0^2}{f(\Theta, Z)} + r_0^2}, f(\Theta, Z) = \left(\frac{\partial \theta}{\partial \Theta}\right)\left(\frac{\partial z}{\partial Z}\right). \tag{5}$$

R_0 is the endocardial radius at ES and r_0 is the endocardial radius at ED. The solutions to $\theta = \theta(\Theta, Z)$ and $z = z(Z)$ can be determined by fitting circumferential and longitudinal displacement data, and are used to predict the radial deformation that is consistent with local geometry (R_0 and r_0), circumferential and axial deformation, and myocardial incompressibility.

2.2 Mouse Heart Imaging and Motion Estimates

Short-axis (SA) and long-axis (LA) cine B-mode images of 6 healthy male C57BL/6 mice (10- to 12- weeks old, 24 to 26 g) were acquired using a VisualSonics Vevo2100 scanner (Toronto, Ontario, Canada) with a MS400 transducer operating at 30 MHz. Imaging frame rate was approximately 350 fps, and the average heart rate of mice under anesthesia was 462±14 bpm. Serial SA images were acquired at 0.5 mm interval, with 10 to 12 slices throughout the LV for each mouse. One LA cine loop through the major axis of the LV was acquired for each mouse.

Displacement fields across the myocardium were determined by speckle tracking with approximately 0.2 mm × 0.2 mm pixel block size using a minimum sum absolute difference (MSAD) algorithm and parabolic fit derived sub-pixel resolution [21]. Displacement components were transformed into cylindrical polar coordinates and fitted to the model.

2.3 Optimization of Model Parameters

For normal mouse hearts, a linear relationship was observed between θ and Θ, and between z and Z. From this observation, the final system of equations is expressed as follows:

$$r(R,\Theta,Z)=\sqrt{\frac{R^2-R_0^2}{ac}+r_0^2},\theta(\Theta,Z)=a\Theta+\tau Z+b,z(Z)=cZ+d. \quad (6)$$

In diseased mouse hearts, higher order polynomials or piece-wise functions might better explain the motions in circumferential and longitudinal directions. For healthy mouse hearts, the constants a, b, c, and d can be determined using linear regression on the observed displacement data in the circumferential and longitudinal directions; however, these constants, specifically a and c, do not optimize the model as a whole, since errors in the radial direction are not taken into consideration. To optimize these constants, the normalized root mean square error (NRMSE) between observed, (r_i,θ_i,z_i), and predicted, $(\hat{r_i},\hat{\theta_i},\hat{z_i})$, position after deformation in each direction is calculated:

$$NRMSE=\frac{1}{3\sqrt{n}}\sum_{x\in(r,\theta,z)}\frac{\sqrt{\sum_{i=1}^{n}(x_i-\hat{x_i})^2}}{x_{max}-x_{min}}. \quad (7)$$

The combination of parameter values that yields the minimum NRMSE is determined to be the optimal values:

$$(a,b,c,d,\tau)=\arg\min(NRMSE(a,b,c,d,\tau)). \quad (8)$$

3 Results

Motions in the circumferential and longitudinal directions were modeled using linear functions. Longitudinal motion is obtained using lateral displacement data derived from tracking LA cine loops. The 0 mm-position is defined at the apex at ES. As shown in figure 1A, tissues that are slightly above the apex did not have any longitudinal displacement, while tissues at the basal level move upward and tissues at the apical level move slightly downward. This effectively results in LV extension. Circumferential motion is illustrated in figure 1B. The 0-rad reference is defined at the section between the papillary muscles, and increases in counterclockwise direction. A difference in phase shift is observed at different levels of the LV. Using the midventricular layer as a reference, the basal and apical layers are observed to rotate in opposite directions. This results in LV torsion.

The coefficients determined using linear regression are optimized in their respective components. Therefore, they are not necessarily optimal for the system. Since b, d, and τ are not used in $r(R, \Theta, Z)$, these parameters can be easily optimized individually after a and c are optimized for the system. A range of values in the neighborhood of the regression coefficients a and c are simulated using the model, and the NRMSE of each combination are shown in figure 2. These coefficients were determined individually for each mouse. A statistical summary of the mean and standard deviation of the values for these coefficients are reported in table 1.

The NRMSE of the system using the optimized value is 4.4±1.2%, represented by the minimum value of the surface in figure 2. Figure 3 shows predicted radial motion at different levels of the LV. The fact that the model captures radial motion at different SA levels with a single choice of parameters for $\partial\theta/\partial\Theta$ and $\partial z/\partial Z$ suggests that most of the variation in radial motion in the normal mouse heart arises from spatial variation in geometry (R_0 and r_0 in equation (6)). As shown in figure 3C, the apical section contributes most of the error; this error near the apex is largely due to tracking error, as shown in the sparsely observed data in figure 3C.

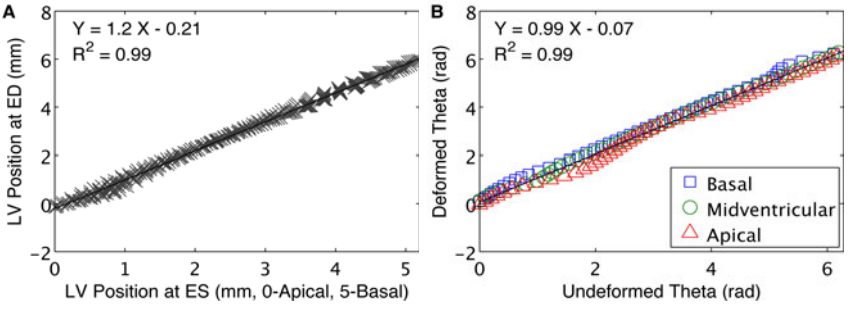

Fig. 1. Linear regression of LV wall motion in longitudinal (A) and circumferential (B) directions. LV extension and torsion are observed, where motions at the basal and apical layers are moving in opposite directions in both components.

Table 1. Optimized values for model Parameters

Parameter	Value
a	1.03±0.12
b	-0.09±0.04 rad
c	1.12±0.08
d	-0.18±0.03 mm
τ	-0.01±0.004 rad/mm

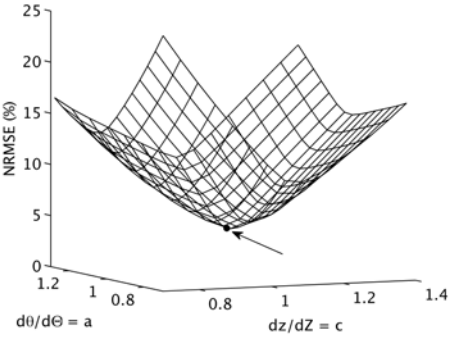

Fig. 2. Model simulation using different combinations of a and c. The NRMSE is calculated for each simulation and the combination with the minimum NRMSE (*arrow*) represents the optimal parameter values.

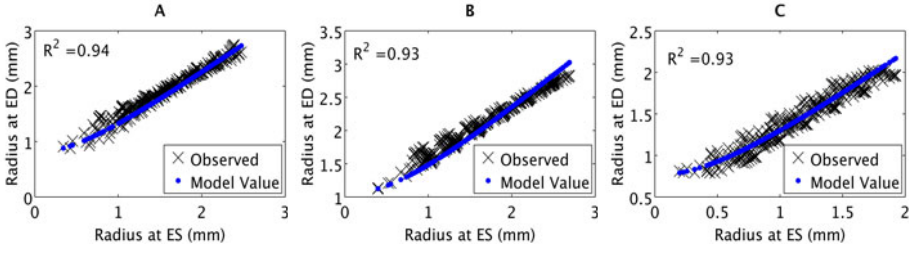

Fig. 3. Observed and predicted radial motion at the base (A), midventricular (B) and apical (C) levels of the LV

4 Conclusion

A unique kinematic model of mouse LV has been shown to accurately predict the motions of the myocardium by enforcing myocardial incompressibility. Compared to a standard cylindrical model, our generalized model can be extended to allow sufficient spatial variation in radial motion to model diseased hearts. In situations with substantial regional variation in deformation, a linear fit will not capture motion in the circumferential component; instead, higher order polynomials or piecewise functions can be used. In these cases, the value for parameter is no

longer a constant, and therefore asymmetric motion can be modeled. Asymmetric motion in the LV can be used to describe the dyssynchrony that is associated with diseased hearts.

Compared to existing geometric models of the LV, the model presented here is simple, and also accurate with 4.4% NRMSE. The presented model is shown to work well with ultrasound datasets. This model offers a lower cost approach to patient-specific modeling by using relatively noisy ultrasound image data as opposed to more expensive imaging modalities.

Acknowledgements. This work was supported by NIH NIBI grant EB001826.

References

1. Roger, V.L., Go, A.S., Lloyd-Jones, D.M., Adams, R.J., Berry, J.D., Brown, T.M., Carnethon, M.R., Dai, S., de Simone, G., Ford, E.S., Fox, C.S., Fullerton, H.J., Gillespie, C., Greenlund, K.J., Hailpern, S.M., Heit, J.A., Ho, P.M., Howard, V.J., Kissela, B.M., Kittner, S.J., Lackland, D.T., Lichtman, J.H., Lisabeth, L.D., Makuc, D.M., Marcus, G.M., Marelli, A., Matchar, D.B., McDermott, M.M., Meigs, J.B., Moy, C.S., Mozaffarian, D., Mussolino, M.E., Nichol, G., Paynter, N.P., Rosamond, W.D., Sorlie, P.D., Stafford, R.S., Turan, T.N., Turner, M.B., Wong, N.D., Wylie-Rosett, J.: Heart Disease and Stroke Statistics 2011 Update: A Report From the American Heart Association. Circulation 123, e18–e209 (2011)
2. Taylor, C.A., Figueroa, C.A.: Patient-specific Modeling of Cardiovascular Mechanics. Annu. Rev. BioMed. Eng. 11, 109–134 (2009)
3. Mihalef, V., Ionasec, R., Wang, Y., Zheng, Y., Georgescu, B., Comaniciu, D.: Patient-specific Modeling of Left Heart Anatomy, Dynamics and Hemodynamics from High Resolution 4D CT. In: IEEE ISBI, pp. 504–507 (2010)
4. Niederer, S., Rhode, K., Razavi, R., Smith, N.: The Importance of Model Parameters and Boundary Conditions in Whole Organ Models of Cardiac Contraction. In: Ayache, N., Delingette, H., Sermesant, M. (eds.) FIMH 2009. LNCS, vol. 5528, pp. 348–356. Springer, Heidelberg (2009)
5. Humphrey, J.D., Yin, F.C.: Constitutive Relations and Finite Deformations of Passive Cardiac Tissue II: Stress Analysis in the Left Ventricle. Cir. Res. 65, 805–817 (1989)
6. Guccione, J.M., McCulloch, A.D., Waldman, L.K.: Passive Material Properties of Intact Ventricular Myocardium Determined From a Cylindrical Model. J. Biomech. Eng. 113, 42–55 (1991)
7. Arts, T., Hunter, W.C., Douglas, A.D., Muijtjens, A.M., Reneman, R.S.: Description of the Deformation of the Left Ventricle by a Kinematic Model. J. Biomechanics 25, 1119–1127 (1992)
8. Costa, K.D., Hunter, P.J., Rogers, J.M., Guccione, J.M., Waldman, L.K., McCulloch, A.D.: A Three-Dimesional Finte Element Method for Large Elastic Deformations of Ventricular Myocardium: I–Cylindrical and Spherical Polar Coordinates. J. Biomech. Eng. 118, 452–463 (1996)
9. Garson, C.D., Li, B., Acton, S.T., Hossack, J.A.: Guiding Automated Left Ventricular Chamber Segmentation in Cardiac Imaging Using the Concept of Conserved Myocardial Volume. Comp. Med. Imag. Graph 32, 321–330 (2008)

10. Zhu, Y., Papademetris, X., Sinusas, A.J., Duncan, J.S.: A Coupled Deformable Model for Tracking Myocardial Borders from Real-time Echocardiography Using an Incompressibility Constraint. Med. Image Analysis 14, 429–448 (2010)
11. Bistoquet, A., Oshinski, J., Skrinjar, O.: Myocardial Deformation Recovery from Cine MRI Using a Nearly Incompressible Biventricular Model. Med. Image Analysis 12, 69–85 (2008)
12. Mansi, T., Pennec, X., Sermesant, M.: iLogDemons: A Demons-Based Registration Algorithm for Tracking Incompressible Elastic Biological Tissues. Int. J. Comput. Vis. 92, 92–111 (2010)
13. Wang, Y., Georgescu, B., Comaniciu, D., Houle, S.: Learning-Based 3D Myocardial Motion Flow Estimation Using High Frame Rate Volumetric Ultrasound Data. In: IEEE ISBI, pp. 1097–1100 (2010)
14. Lediju, M.A., Pihl, M.J., Hsu, S.J., Dahl, J.J., Gallippi, C.M., Trahey, G.E.: A Motion-Based Approach to Abdominal Clutter Reduction. IEEE Trans. Ultrason. Ferro. Freq. Cont. 56, 2437–2449 (2009)
15. Gallippi, C.M., Trahey, G.E.: Adaptive Clutter Filtering Via Blind Source Separation for Two-Dimensional Ultrasonic Blood Velocity Measurement. Ultrason. Imag. 24, 193–214 (2002)
16. Adkins, J.E.: Some General Results in the Theory of Large Elastic Deformation. Proc. R. Soc. 231, 75–90 (1955)
17. Spencer, A.J.M.: Continuum Mechanics. Longman Press, London (1980)
18. Aliev, M.K., Santos, P.D., Hoerter, J.A., Soboll, S., Tikhonov, A.N., Saks, V.A.: Water Content and Its Intracellular Distribution in Intact and Saline Perfused Rat Hearts Revisited. Cardio. Res. 53, 48–58 (2002)
19. Vinnakota, K.C., Bassingthwaighte, J.B.: Myocardial Density and Composition: A Basis for Calculating Intracellular Metabolite Concentrations. Am. J. Physiol. Heart Circ. Phyiol. 286, H1742–H1749 (2004)
20. Judd, R.M., Levy, B.I.: Effects of Barium-induced Cardiac Contraction on Large- and Small-Vessel Intramyocardial Blood Volume. Circulation 68, 217–225 (1991)
21. Li, Y., Garson, C.D., Xu, Y., Beyers, R.J., Epstein, F.H., French, B.A., Hossack, J.A.: Quantification and MRI Validation of Regional Contractile Dysfunction in Mice Post Myocardial Infarction Using High Resolution Ultrasound. Ultrasound in Med. & Biol. 33, 894–904 (2007)